ACS APPLIED MATERIALS & INTERFACES
Research Article
www.acsami.org

Dual Responsive Enzyme Mimicking Activity of AgX (X = Cl, Br, I) Nanoparticles and Its Application for Cancer Cell Detection

Guang-Li Wang,*[†,‡] Xiu-Fang Xu,[†] Ling Qiu,[§] Yu-Ming Dong,[†] Zai-Jun Li,[†] and Chi Zhang[†]

[†]The Key Laboratory of Food Colloids and Biotechnology, Ministry of Education, School of Chemical and Material Engineering, Jiangnan University, Wuxi 214122, P. R. China

[‡]State Key Laboratory of Analytical Chemistry for Life Science, Nanjing University, Nanjing 210093, P. R. China

[§]Key Laboratory of Nuclear Medicine, Ministry of Health and Jiangsu Key Laboratory of Molecular Nuclear Medicine, Jiangsu Institute of Nuclear Medicine, Wuxi 214063, P. R. China

Supporting Information

ABSTRACT: Chitosan (CS) modified silver halide (AgX, X = Cl, Br, I) (CS-AgX) nanoparticles (NPs) were found to possess dual responsive enzyme mimetic activities. In the presence of H_2O_2, they were able to oxidize various colorimertic dyes, namely, peroxidase-like activity. Upon photoactivation, CS-AgX NPs could also oxidize the typical substrates in the absence of H_2O_2. Taking CS-AgI as an example, it was found that the photostimulated enzyme mimetics of CS-AgI NPs showed several unprecedented advantages over natural peroxidase or other existing alternatives based on nanomaterials, such as excellent enzyme-like activity over a broad pH range (3.0−7.0), the independence of hydrogen peroxide on activity, the easily regulated activity by light irradiation, and the good reutilization without significant loss of catalytic activity. The mechanism of the dual responsive enzyme-like activity of CS-AgI was investigated. On the basis of these findings, the photoactivated CS-AgI was designed to develop a facile, cheap, rapid, and highly sensitive colorimetric assay to detect cancer cells. The detection limit of the method for MDA-MB-231 was estimated to be as low as 100 cells, which was much lower than that reported by the method using peroxidase mimetics based on nanomaterials. We believe that CS-AgX NPs with dual responsive enzyme-mimicking activity, especially the excellent photostimulated enzyme-like activity, may find widely potential applications in biosensors.

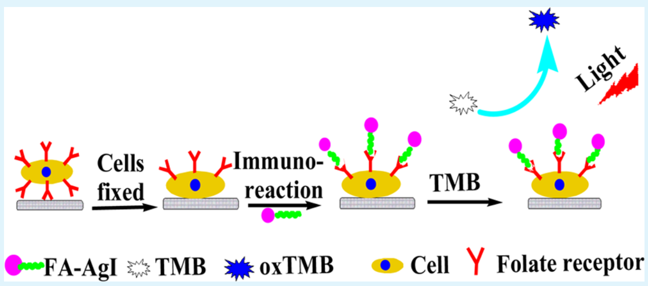

KEYWORDS: *enzyme mimetics, silver halides nanoparticles, cancer cell detection, light irradiation, chitosan, catalytic activity*

INTRODUCTION

Owing to their efficient catalytic power and high substrate specificity, natural enzymes have been attracting great interest in various fields including pharmaceutical processes, biosensing, agrochemical production, and food industry applications.[1,2] However, problems such as sensitivity of catalytic activity to environmental conditions, low operational stability due to denaturation and digestion as well as high cost in preparation and purification largely limit their applications.[3] For example, in traditional enzyme linked immunosorbent assays (ELISA), a horseradish peroxidase (HRP)-labeled secondary antibody is utilized to assess the binding of a specific primary antibody to a particular target or surface receptor. This binding event is assessed by the ability of HRP to oxidize a chromogenic substrate such as 3,3′,5,5′-tetramethylbenzydine (TMB) in the presence of hydrogen peroxide. However, due to the instability of HRP, in addition to the H_2O_2-induced inactivation of bimolecular, this method often exhibits a high rate of erroneous results.[4] Thus, developing enzyme mimetics is highly appealing.[5] Especially, the rapidly growing field of nanotechnology provides excitingly new possibilities for the development of enzyme mimics. Since the pioneering work using Fe_3O_4 as peroxidase mimetics,[4] enzyme mimetics based on nanomaterials have received great attention. Subsequently, different nanostructures including graphene oxide,[6] composite of graphene oxide and gold nanoclusters,[7] single-walled or helical carbon nanotubes,[8,9] carbon nanodots,[10] metal oxides,[11−13] and metallic[14] or bimetallic nanostructures[15] were found to possess peroxidase-like activity, which could catalyze the oxidation of the typical organic chromogenic substrates using hydrogen peroxide as an oxidant. Compared to natural enzymes, nanomaterials may serve as promising candidates for artificial enzymes, due to several advantages, including low cost, tunability in catalytic activities, improved stability, and ease of storage and treating.[16]

Interestingly, some nanostructures were found to have dual enzyme-like activities. For example, Au@Pt[17] and BSA-templated MnO_2 nanostructures[18] were found to behave as

Received: December 21, 2013
Accepted: April 22, 2014
Published: April 22, 2014

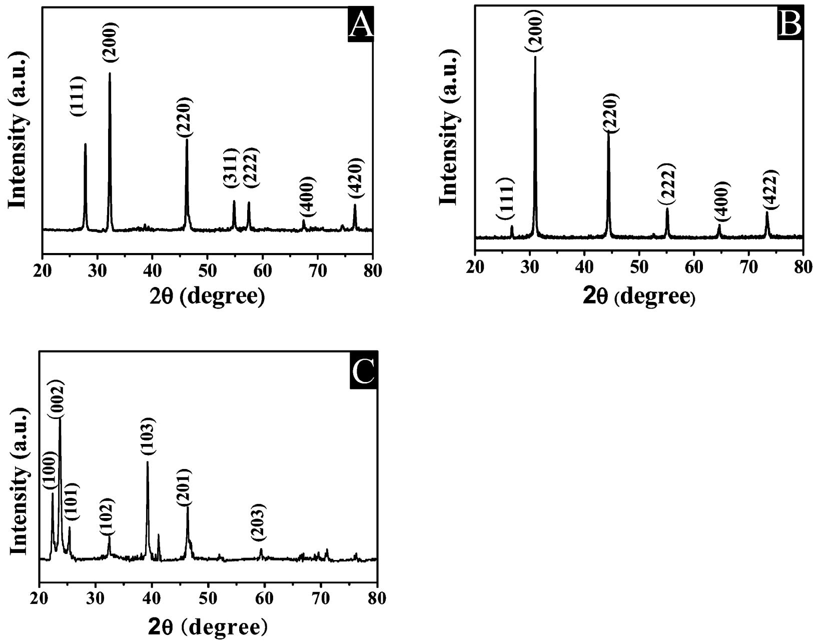

Figure 1. XRD patterns of the as-prepared samples: (A) CS-AgCl, (B) CS-AgBr, and (C) CS-AgI.

both oxidase and peroxidase mimetics. Co_3O_4 nanoparticles[13] and silicon nanowires[19] were found to possess intrinsic peroxidase-like activity and catalase-like activity. In this Article, excitingly, we found that chitosan (CS) modified silver halide (AgX, X = Cl, Br, I) (CS-AgX) nanoparticles (NPs) possessed dual responsive enzyme mimetic activities. In the presence of hydrogen peroxide, CS-AgX NPs catalyzed the oxidation of the typical substrates of peroxidase (including o-phenylenediamine-(OPD), 3,3′,5,5′-tetramethylbenzydine (TMB), and 2,2-azinobis(3-ethylbenzothizoline-6-sulfonic acid) (ABTS)), exhibiting peroxidase-like activity. Under visible-light ($\lambda \geq 420$ nm) stimulation, the CS-AgX NPs also demonstrated the same enzyme-like activity in the absence of H_2O_2. It should be emphasized that the photostimulated CS-AgX NPs showed surprisingly high enzyme-like activity over a broad pH range (3.0−7.0) even at neutral pH, which overcomes one of the main shortcomings that currently developed enzyme mimics suffer when they are applied in biological systems (their optimum reaction activity occurs in strongly acidic solution with a pH below 4.0, which is not in accordance with the activity of the pH-labile biomolecules where a near neutral pH is required). In addition, the photostimulated CS-AgX NPs demonstrated enzyme-like activity in the absence of the destructive hydrogen peroxide, indicating its better biocompatibility for promising applications in vivo.[20,21] A different catalytic mechanism was found for the enzyme-like activity of CS-AgI NPs in the presence of hydrogen peroxide or visible light activation. The photoactivated CS-AgI NPs possessing enzyme-like activity were applied as robust nanoprobes for sensitive, selective, and fast colorimetric detection of cancer cells. We expect that CS-AgX NPs can become a novel substitute for natural enzyme with great potential in bioanalytical chemistry.

■ EXPERIMENTAL SECTION

Materials and General Instruments. Silver nitrate, chitosan-(CS), *o*-phenylenediamine (OPD), 2,2′-azino-bis(3-ethylbenzo-thiazoline-6-sulfonic acid) diammonium salt (ABTS), 3,3,5,5-tetramethylbenzidine(TMB), *t*-butanol, *p*-benzoquinone, isopropanol, H_2O_2, acetic acid, sodium acetate, KCl, KBr, KI, and folic acid (FA) were purchased from Sinopharm Chemical Reagent Co., Ltd. (Shanghai,China). 1-Ethyl-3(3-(dimethylamino)propyl) carbodiimide hydrochloride (EDC), *N*-hydroxysulfosuccinimide sodium (sulfo-NHS), and 2-(*N*-morpholino) ethanesulfonic (MES) acid sodium salt were purchased from Sigma. All other chemicals used were of analytical grade. All solutions were prepared with ultrapure water (18.2 M cm^{-1}) obtained from a Healforce water purification system.

X-ray diffraction (XRD) measurement was carried out at room temperature using a X-ray powder diffractometer with Cu Kα radiation (λ = 0.154178 nm) and a scanning speed of 4°/min (Brooke AXS, Germany). Transmission electron microscopy (TEM) images of CS-AgX were obtained on a JEOL JEM-2100 transmission electron microscope (Hitachi, Japan). UV−vis absorption spectroscopic measurements were carried out using a TU-1901 spectrophotometer (Beijing Purkinje General Instrument Co., Ltd., Beijing, China). Fluorescence spectra were measured on a Cary Eclipse fluorescence spectrophotometer (Varian Co., LTD). Photoelectrochemical measurements were performed with a homemade photoelectrochemical system. A 500 W Xe lamp (Au Light Source, Beijing) equippped with an ultraviolet cutoff filter ($\lambda \geq 420$ nm) was used as the irradiation source, and the light intensity were fixed at 66.1 mW/cm^2 (the light intensity was estimated by using a FieldMax II-Top power meter (Coherent)). Photocurrent was measured on a CHI 800C electrochemical workstation. CS-AgI NPs modified ITO electrode with an area of 0.25 cm^2 was employed as the working electrode. A Pt wire was used as the counter electrode and a saturated Ag/AgCl as the reference electrode. All the photocurrent measurements were performed at a constant potential of 0 V (vs saturated Ag/AgCl). A 0.1 mol/L Na_2SO_4 solution was used as the supporting electrolyte for photocurrent measurements. FTIR spectra were recorded an ABB Bomem FTLA 2000-104 spectrometer (ABB Bomem, Canada) in the transmission mode using KBr pellets of the sample. Pictures of cells were taken on inverted fluorescence microscope (Olympus BX-51, Japan). The detection of cells by absorption method was conducted on 96 well plates by Enzymelabeled meter (Multiskan MK3: Thermo-labsystems). The pH of the HAc-NaAc buffer solution was measured with a glass electrode connected to a PHS-3C pH meter (Shanghai, China).

Synthesis of CS-Functionalized Silver Halides (AgX) NPs. In a typical procedure, CS-AgX (X = Cl, Br, I) nanoparticles were prepared by a precipitation method. Briefly, 20 mL of 0.1 M $AgNO_3$ aqueous solution was mixed with 20 mL of 0.5% (m/v) chitosan solution and stirred for 30 min, then 20 mL of 0.15 M KX (X = Cl, Br, I) aqueous solution were added into the above solution and stirred for 3 h. After that, a dispersion containing CS-AgX nanoparticles was formed.

Conjugation of Folic Acid to CS-AgI. To conjugate the CS-AgI with folic acid (FA), free folic acid (20 mg, 0.0227 mmol) was first dissolved in 10 mL 50 mM MES buffer (pH 6.0). The solution of FA was then mixed with a 2 mL aqueous solution of (EDC) (10 mmol) and sulfo-NHS (10 mmol). After agitating overnight at room temperature in the dark, the solution of CS-AgI (10 mL) was added to the above mixture. The resulting solution was stirred at room temperature for 24 h. The final reaction mixture was purified by dialysis using 3500 molecular weight cut off dialysis bag, against ultrapure water to remove the residual impurities.

Procedure for the Oxidation of the Substrates by H_2O_2 Using CS-AgI as Catalysts. To investigate the peroxidase-like activity of the as-prepared CS-AgI, the catalytic oxidation of the peroxidase substrate TMB in the presence of H_2O_2 was tested. Experiments were carried out using 51 μg/mL CS-AgI in a reaction volume of 5 mL acetate buffer solution (40 mmol/L, pH 4.0) with 60 μmol/L TMB as substrate, and the H_2O_2 concentration was 10 mmol/L, unless otherwise stated.

To examine the influence of reaction buffer pH incubation temperature on the peroxidase-like activity of CS-AgI, 0.2 M acetate buffer solutions from pH 2.5 to 11.0 and different temperature water baths from 20 to 60 °C were investigated.

Process of Oxidation of Substrates under Visible Light Irradiation ($\lambda \geq 420$ nm). To examine the capability of CS-AgI as a catalyst on the oxidation of TMB under visible light irradiation ($\lambda \geq 420$ nm), Experiments were carried out using 51 μg/mL CS-AgI in a reaction volume of 5 mL of acetate buffer solution (40 mmol/L, pH 4.0) with 60 μmol/L TMB as substrate. The above solution was irradiated with a 300 W Xe lamp equipped with an ultraviolet cutoff filter ($\lambda \geq 420$ nm) to provide visible light at room temperature.

Immunoassays for Cancer Cells. All cell lines including breast cancer cells (MDA-MB-231), human liver carcinoma cells (Hep G2), lung adenocarcinoma cells (A549) and human normal liver cells (L02) were grown in Iscove's modified Dulbecco's medium supplemented with 1% penicillin-streptomycin solution and 10% fetal calf serum in a humidified 37 °C incubator with 5% CO_2. Cells were plated in 96-well plates and fixed after 24 h incubation, and then they were incubated with 100 μL 440 μg/mL FA-CS-AgI NPs for 3 h. Afterward, cells were washed by phosphate buffer (pH = 7.0) three times and then 100 μL 0.5 mM TMB was added. The plate was illuminated under visible light irradiation ($\lambda \geq 420$ nm) for 10 min to allow development of the blue color. The absorbance of the oxidation product was monitored at 652 nm with a microplate reader.

RESULTS AND DISCUSSION

Characterization of Enzyme-like Activity of CS-AgX Nanostructures. The X-ray powder diffraction (XRD) patterns of the as-synthesized silver halides (CS-AgX) samples are shown in Figure 1. It is observed that all the peaks of the sample coincide with the standard face-centered cubic AgCl (JCPDS file 31-1238), face-centered cubic AgBr (JCPDS file 06-0438), and hexagonal β-AgI phase (JCPDS file 78-1613). The typical TEM images of the CS-AgX nanoproducts demonstrate that they were nanoparticles with diameters of 30−70 nm (Supporting Information Figure S1A). The histogram of the size distribution of CS-AgX is shown in Supporting Information Figure S1B. The mean size of CS-AgCl, CS-AgBr, and CS-AgI was 48.2, 42.6, and 40.0 nm, respectively.

Chitosan (CS), a polyelectrolyte derivative of chitin, is a polysaccharide composed of $\beta(1 \rightarrow 4)$ linked 2-amino-2-deoxy-β-D-glucopyranose (*N*-acetylglucosamine).[22] Because of its nontoxicity, biocompatibility, and easy conjugation with nanomaterials, CS was used as a surface modifier for AgX NPs. Fourier transform infrared (FTIR) spectroscopy of CS modified AgX NPs, such as CS-AgI, revealed the existence of amino groups (3400 cm^{-1}, N−H stretching vibration) and acetylated amino groups (1648 cm^{-1}, carbonyl stretching vibration), suggesting that CS was introduced on the surface of AgI (Supporting Information Figure S2). Compared to CS alone, the spectroscopy of CS-AgI revealed a new absorption peak at around 1560 cm^{-1}, suggesting the formation of an Ag−N bond,[23] possibly indicating the means of attachment of CS to AgI.

To investigate the catalytic activity of CS-AgX NPs, we chose 3,3,5,5-tetramethylbenzdine (TMB), *o*-phenylenediamine (OPD), and 2,2-azino-bis(3-ethylbenzothiazoline-6-sulfonic acid) (ABTS) as typical chromogenic substrates, which have been used to demonstrate the oxidase- or peroxidase-like activities of natural enzymes or enzyme mimetics.[4,11,17] It was found that the CS-AgX NPs catalyze the oxidation of TMB, OPD, and ABTS by hydrogen peroxide, producing the typical yellow color for OPD, blue color for TMB, and green color for ABTS (Figure 2) within 30 min. In contrast, the solutions without CS-AgX nanostructures show almost no color change, which supports the conclusion that the CS-AgX nanostructures have peroxidase-like activity. We also found that, under photostimulated CS-AgX in the absence of hydrogen peroxide, the color evolutions of OPD, ABTS, and TMB oxidation are much faster (within 5 min) and exhibit the typical colors (Figure 2). Similarly, control experiments without CS-AgX nanostructures or with CS-AgX in the absence of visible-light illumination show negligible color variation. This indictes that the photoactivated CS-AgX NPs also possess enzyme-like activity even without H_2O_2. The corresponding enzyme-like oxidation reaction of the substrates including TMB,[24] OPD,[19] and ABTS[25] are shown in eq 1. All these above results indicate that the CS-AgX NPs demonstrate dual responsive enzyme-like activity: they can utilize H_2O_2 as an electron acceptor or undergo visible-light stimulation toward oxidization of the typical enzyme substrates.

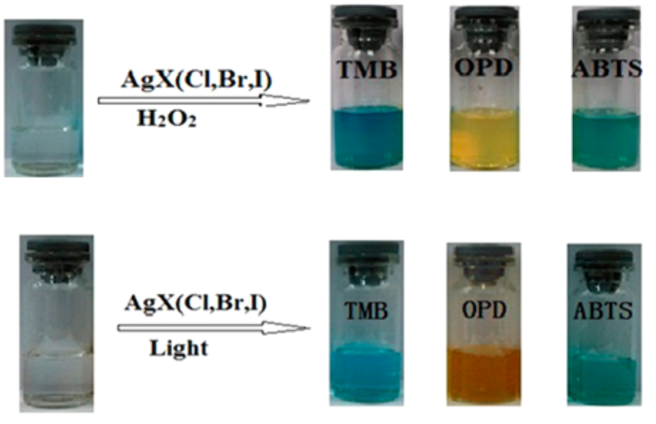

Figure 2. Color evolution of TMB, OPD, and ABTS oxidation by H_2O_2 using CS-AgX (X = Cl, Br, I) as catalysts (top) and visible light stimulated CS-AgX (X = Cl, Br, I) (bottom).

Using TMB as a typical substrate, the catalytic activity of the as-synthesized three different CS-AgX (X = Cl, Br, and I) nanostructures were investigated. The colorless TMB can be oxidized by natural enzymes or enzyme mimetics to its distinctive blue charge-transfer complexes of diamine and diimine with characteristic absorption peaks at 370 and 652 nm

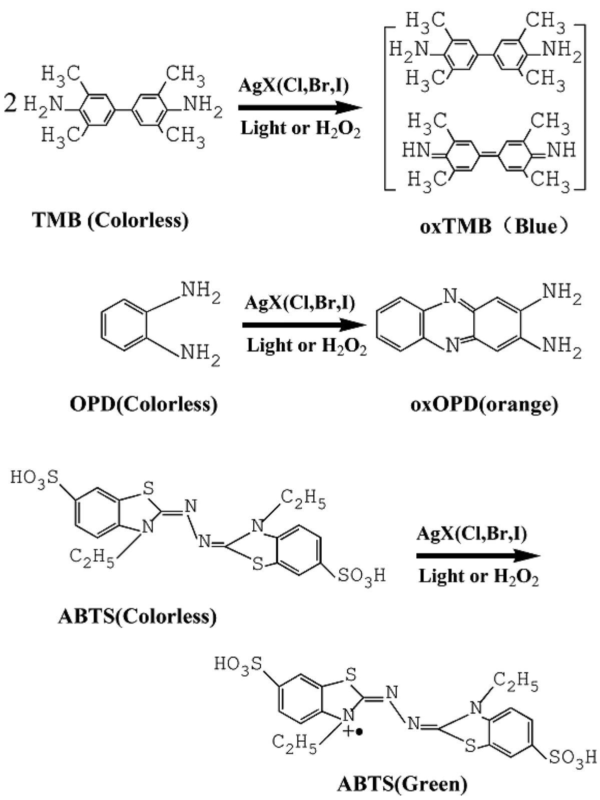

(1)

(Figure 3).[24] The oxidation process of TMB was quantitatively monitored using UV−vis spectrometry (using the maximum wavelength, λ_{max}, of the oxidized state of TMB at 652 nm). It was found that CS-AgI shows a higher activity than that of CS-AgCl and CS-AgBr in H_2O_2 oxidation system using CS-AgX as catalysts and photostimulated CS-AgX (Supporting Information Figure S3). Thus, in the following experiment, we chose CS-AgI as a typical enzyme mimetic for TMB oxidation. Time-dependent absorbance changes at 652 nm revealed the CS-AgI concentration dependent catalytic rate and activity (Supporting Information Figure S4). The catalytic rate and activity increased with the increased concentration of CS-AgI NPs.

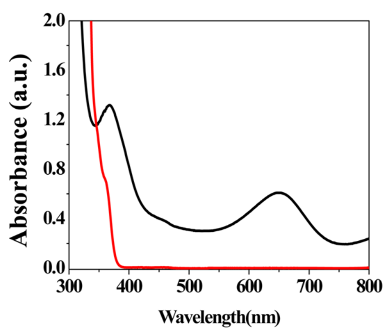

Figure 3. UV−vis spectra of TMB before (red line) and after (black line) oxidation by H_2O_2 using CS-AgX (X = Cl, Br, I) as catalysts or visible light stimulated CS-AgX (X = Cl, Br, I).

Similar to natural enzymes, the peroxidase mimetics based on CS-AgI NPs showed pH, temperature, and H_2O_2 concentration dependent catalytic activities (Figure 4). For the catalytic oxidation of TMB by hydrogen peroxide using CS-AgI as catalyst, the optimal pH is ca. 4.0 and an optimal temperature is 35 °C. For peroxidase-like activity, as expected, a strong dependence was found between initial reaction rate and H_2O_2 concentration. The response may be potentially used to fabricate a detection platform for H_2O_2-related processes such as substrate (glucose, xanthine, choline, etc.) oxidation by the corresponding oxidase to produce H_2O_2.[6,26,27] For further acquiring kinetic parameters, the catalytic activities of CS-AgI for the oxidation of TMB at pH 4.0 using H_2O_2 as electron acceptor were studied by enzyme kinetics theory and methods. The kinetic data were obtained by changing one substrate concentration and fixing that of the other substrate. Typical Michaelis−Menten curves were received in a certain range of the substrate (TMB or H_2O_2) concentration (Supporting Information Figure S5). According to the function, the apparent kinetic parameters were calculated using the equation $\nu = V_{max}[S]/(K_m + [S])$, where ν, V_{max}, [S], and K_m refer to the initial enzymatic reaction rate, the maximum enzymatic reaction rate, the concentration of the substrate, and the Michaelis constant, respectively. This is a good indication that the catalytic process obeys the Michaelis−Menten kinetics.[28] Compared with that of HRP (K_m = 0.434 mM for TMB and 3.7 mM for H_2O_2),[4] the K_m values of CS-AgI with TMB (K_m = 0.0238 mM) or H_2O_2 (K_m = 2.86 mM) as the substrate are lower, indicating that CS-AgI has a higher affinity for TMB or H_2O_2 than HRP.

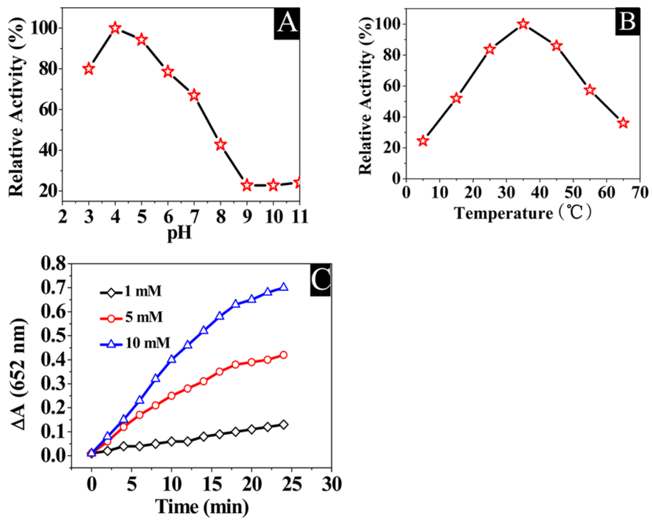

Figure 4. The catalytic activity of CS-AgI NPs is dependent on pH (A), temperature (B) and H_2O_2 concentration (C). Reaction conditions: 60 μM TMB, 51 μg/mL CS-AgI.

The most exciting feature of the enzyme-like activity of the photoactivated CS-AgI was that it exhibited high catalytic activity over a broad pH range (3.0−7.0), even at neutral pH (Figure 5A). This feature was distinctly superior to that of the natural peroxidase or peroxidase mimetics based on nanomaterials, which showed very low activity at neutral pH.[6,10,29,30] The low activity of the natural peroxidase or peroxidase mimetics based on nanomaterials at neutral pH is not in accordance with the activity of the pH-labile biomolecules where a near neutral pH is required, greatly limiting their application in biological systems. CS-AgX NPs with excellent photostimulated enzyme like activity may open a new avenue for the design and application of enzyme mimetis in biosensors. The photostimulated enzyme-like activity of CS-AgI was relatively higher and stable in the temperature range of 25−45 °C (Figure 5B). The good stability and high catalytic activity of the photostimulated CS-AgI in the temperature range of 25−

dx.doi.org/10.1021/am501830v | ACS Appl. Mater. Interfaces 2014, 6, 6434−6442

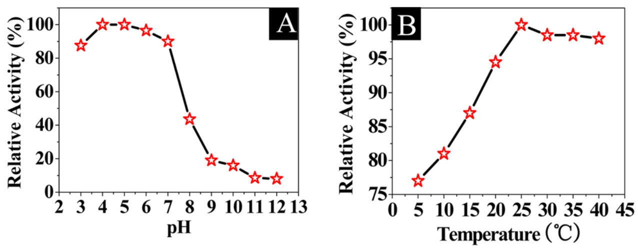

Figure 5. Relative catalytic activity of the CS-AgI NPs under visible light irradiation ($\lambda \geq 420$ nm) at a range of different solution pH (A) and different reaction temperatures (B). Reaction conditions: 60 μM TMB, 51 μg/mL CS-AgI.

45 °C demonstrated that it is a promising candidate in biosensing. In addition, it was found the photoactivated enzyme-like activity of CS-AgI could be easily regulated by tuning the light intensity. If the light intensity increased, the photoactivated enzyme-like activity of CS-AgI also increased. Kinetic studies of oxidation of TMB by phtoactivated CS-AgI at neutral pH (pH 7.0) was found to also obey the typical Michaelis–Menten mechanism (Supporting Information Figure S6). The apparent K_m and the maximum rate value of CS-AgI with TMB as substrate was 22.8 μM and 169 nM S^{-1}, respectively. The apparent K_m of the photoactivated CS-AgI at neutral pH is comparable with its activity using H_2O_2 as an oxidant at pH 4.0 but much lower than that of HRP at the same condition (0.20 mM).[7] In addition, it was found that the photostimulated catalytic activity of CS-AgI remained 95% after five catalytic cycles (Supporting Information Figure S7). Still, this highlights the excellent catalytic properties of the photoactivated CS-AgI NPs for TMB oxidation. It is well-known that the extent of bioapplicability of the enzyme mimics depends strongly upon their stability and catalytic activity in solutions at mild conditions. Because of their excellent enzyme-like catalytic activity at neutral pH without H_2O_2, as well as good stability, the photostimulated CS-AgI NPs are promising candidates to be used widely in biological systems.

In order to elucidate the catalytic mechanism of CS-AgI in the presence of H_2O_2 and under illumination, a series of quenchers were employed to scavenge the relevant reactive species including hydroxyl radicals (${}^{\bullet}OH$), superoxide anions ($O_2^{\bullet-}$), photogenerated holes (h^+) of photoactive materials, etc. Here, isopropanol or tert-butanol was used to quench ${}^{\bullet}OH$ in solution.[31,32] As shown in Supporting Information Figure S8, isopropanol or *t*-butanol quencher exhibits a slight depression in the catalytic activity of CS-AgI using H_2O_2 as electron acceptor while they have almost no influence on the oxidation of TMB under photoactivated CS-AgI. This indicates that ·OH was produced due to the interaction between CS-AgI and H_2O_2 but almost no ·OH exist in the solution of illuminated CS-AgI. Terephthalic acid (TA) was also adopted as a fluorescence probe to confirm the generation of ·OH. TA easily reacted with ·OH to form highly fluorescent 2-hydroxy terephthalic acid.[33,34] An emission peak at 425 nm appeared after TA was added in CS-AgI solution in the presence of H_2O_2 (Supporting Information Figure S10), which implied the production of ·OH radicals after the interaction between CS-AgI and H_2O_2. However, no PL signal was observed upon irradiation of the mixture of CS-AgI and TA solution, indicating no production of ·OH radicals for irradiated CS-AgI. Using p-benzoquinone (BQ) as a specific quencher for $O_2^{\bullet-}$ failed in our experiment because all the substrates including OPD, ABTS and TMB reacted with BQ directly.[35,36] By replacing these enzyme substrates with a typical organic dye (methyl orange) often used in evaluating the catalytic performance of photocatalysts[37−39] we found that the introduction of BQ significantly restrains the H_2O_2 or photo-oxidation of methyl orange by CS-AgI (Supporting Information Figure S9), suggesting that $O_2^{\bullet-}$ plays a key role in the enzyme-like oxidation reaction of the above two systems. Nitro Blue Tetrazolium (NBT) can directly react with superoxide anion radical ($O_2^{\bullet-}$) and it can be reduced to formazan with the characteristic maximum absorption peak at 680 nm.[40] As demonstrated in Figure S11 in the Supporting Information, the emergence of the absorption peak of the reduced NBT suggested the generation of $O_2^{\bullet-}$ radicals in the enzyme-like oxidation reaction of the above two systems. For photoactivated CS-AgI NPs, the oxidation rate also exhibit an obvious depression in the presence of EDTA and the inhibition extent increases with the concentration of EDTA (Supporting Information Figure S8). This result indicates that the photogenerated holes (h^+) are also reactive species responsible for TMB oxidation.[41] AgI is a narrow band gap semiconductor. When AgI is exposed to visible light illumination, it absorbs photons and results in the corresponding generation of electrons in the conduction band (CB) and holes (h^+) in the valence band (VB). The valence band potential of AgI was estimated to be above 2.0 eV vs NHE,[42] which was able to oxidize TMB with a redox potential in the range of 0.22 to 0.7 V.[24] Thus, the photogenerated holes can transfer to the surface of AgI and oxidize TMB to oxTMB. Photoelectrochemistry is a useful tool to study photoinduced charge transfer properties of semiconductors.[43,44] The photocurrent of CS-AgI NPs modified indium tin oxide (ITO) electrodes were recorded with CS-AgI under several on/off visible-light ($\lambda \geq 420$ nm) irradiation cycles in 0.1 mol/L Na_2SO_4 solution. The sample promptly generates stable photocurrent with a reproducible response to on/off cycles, demonstrating the effective charge generation and transfer of photoactivated CS-AgI (Supporting Information Figure S12). Besides the photogenerated holes, the photogenerated electrons (e^-) can also participate in the oxidation process through the reduction of the dissolved O_2 in solution to the superoxide radical ($O_2^{\bullet-}$).[45−47] After bubbling the solution with nitrogen to remove dissolved oxygen, the catalytic activity of the photoactivated CS-AgI for TMB oxidation decreases. This also confirms that dissolved O_2 is involved in the photocatalytic reaction. From the above results, we speculated that the dominant reactive species for the oxidation of TMB under illuminated CS-AgI are $O_2^{\bullet-}$ and photogenerated holes (h^+). However, for the H_2O_2 oxidation system using CS-AgI as catalysts, it is possible that CS-AgI NPs activate H_2O_2 to yield active intermediates, including $O_2^{\bullet-}$ and ·OH, which serve as the main active species involved in the oxidation of TMB. The schematic illustration of oxidation of TMB by CS-AgI-H_2O_2 and photoactivated CS-AgI are shown in Scheme 1.

Application in Cancer Cell Immunoassay. The rapid, sensitive, and accurate detection of cancer cells is particularly critical, as it not only can provide an easier and more effective way to monitor progression of the disease, but also facilitates the selection of effective therapeutic pathways and improve clinical outcomes.[48−51] As a proof of concept for biosensing, the photoactivated CS-AgI demonstrating high enzyme-like activity and good stability at neutral pH was used as a robust probe to detect cancer cells. Folic acid (FA), one of the best-

Scheme 1. Process of Oxidation of TMB by CS-AgI-H_2O_2 (A) or by Photoactivated CS-AgI (B)

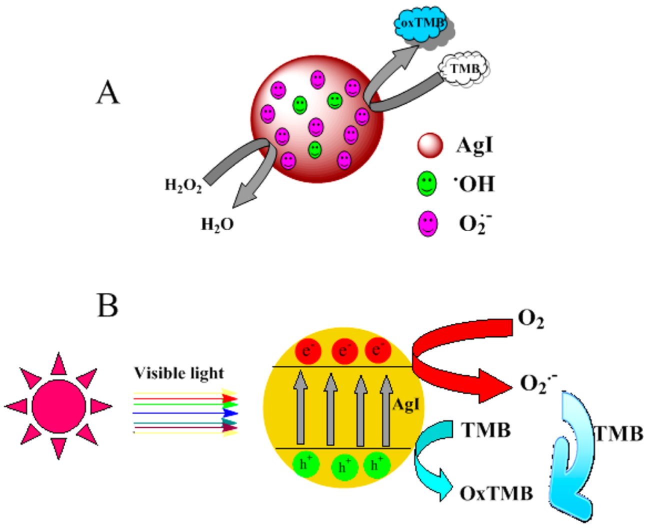

characterized ligands, is widely employed to target tumors or cancer cells because folate receptors usually overexpress on the membrane of many human cancer cells, such as ovarian, endometrial, colorectal, breast, lung, liver, kidney, prostate, renal cell carcinomas, brain metastases derived from epithelial cancers, and neuroendocrine carcinomas cancer cells, and so forth, in contrast to a low expression level in normal cells.[52−54] Due to high-affinity and specificity to folate receptors, FA is a promising targeting agent because of its stability, inexpensiveness, poor immunogenicity, and capability to be conjugated with a wide variety of molecules or nanoparticles. In our experiment, FA-CS-AgI conjugates were synthesized by chemically coupling FA to CS via the formation of an amide bond between the residual amine groups of CS and the carboxyl groups of FA. In the UV−vis spectra, new peaks at 223 and 290 nm appeared due to the presence of FA on CS-AgI (Supporting Information Figure S13), which indicated the conjugation of FA on the surface of CS-AgI. The as prepared FA-CS-AgI was also confirmed by fluorescence spectra. An emission peak at 450 nm, characteristic of FA[55] was observed in the FA-CS-AgI (Supporting Information Figure S14). After cancer cells, such as lung adenocarcinoma cells (A549), were incubated with FA-CS-AgI, yellow spots were found (Figure 6), which indicated that FA-CS-AgI could successfully bind to cancer cells through FA-folate receptors mediated recognition.

The photoactivated FA-CS-AgI with enzyme-like activity was utilized for the quantitative colorimetric detection of cancer cells (as shown in Scheme 2). An increasing number of folate-

Scheme 2. Proposed Detection Process Using FA-CS-AgI[a]

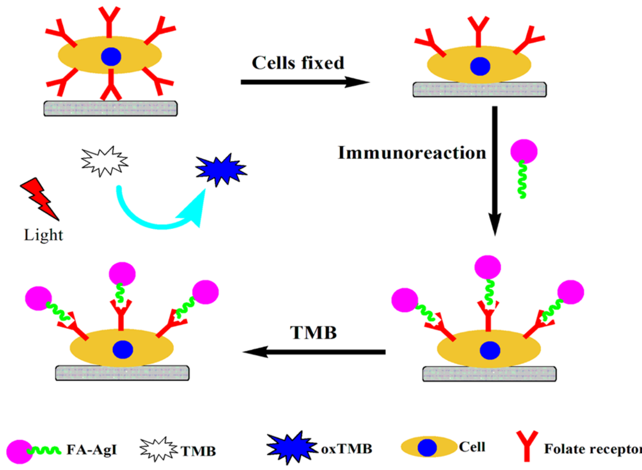

[a]Cells were fixed and treated with FA-CS-AgI nanoparticles for 3 h, and then washed with phosphate buffer (pH = 7) three times. TMB (100 μL, 0.5 mM) was subsequently added and irradiated under visible light irradiation ($\lambda \geq 420$ nm) for 10 min.

positive MDA-MB-231 human breast cancer cells (1000−8000 cells) were treated with a constant amount of FA-CS-AgI (220 μg/mL). In the presence of TMB and after visible-light illumination for 10 min, the AgI-conjugated cells catalyzed a color reaction that can be judged by the naked eye easily and be quantitatively monitored by the absorbance change at 652 nm. An increase in the formation of TMB oxidation product (652 nm absorbance) with increasing number of MDA-MB-231 cells was observed (Figure 7A). This result was expected, as an increasing number of MDA-MB-231 cells translates into an increasing number of surface folate receptors available for binding to the FA-CS-AgI NPs. Using this method, as low as 1000 MDA-MB-231 cells could be visualized clearly by naked-eye, demonstrating good sensitivity of the method. The detection limit was estimated to be 100 cells at 3σ, which was much lower than the detection limit reported by the method using peroxidase mimetics based on nanomaterials.[7]

Catalytic reactions of enzyme labels are usually used in biosensors to generate a large number of signaling species per

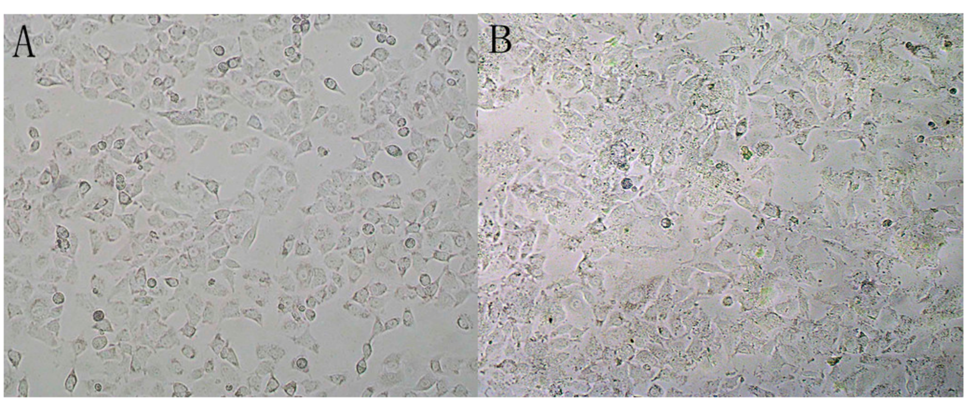

Figure 6. Comparison between A549 cells (A) and the A549 cells after incubation with FA-CS-AgI (B).

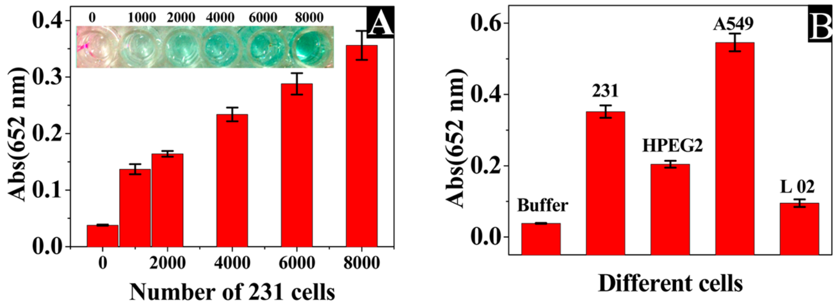

Figure 7. (A) MDA-MB-231 cells were detected by FA-CS-AgI in the presence of TMB under visible light irradiation for 8 min. Inset shows the color change of the different number of cells. (B) Response of different cells using FA-CS-AgI to TMB under visible light irradiation. The error bars represent the standard deviation of five measurements.

target.[56−58] The incubation period for catalytic reactions must be sufficiently long to obtain high signal amplification, that is, low detection limit. An incubation period of 10 min is required in this photoactivated catalytic system, which is shorter than the incubation period of more than 30 min that is generally required for microplate-based ELISAs.

To assess if FA-CS-AgI has specificity to folate receptors, different cell lines are used: breast cancer cells (MDA-MB-231), human liver carcinoma cells (Hep G2), lung adenocarcinoma cells (A549), and human normal liver cells (L02). L02 cells do not overexpress folate receptors, while the other cell lines do. FA-CS-AgI showed much stronger binding to cancer cells (MDA-MB-231, Hep G2, and A549 cells) than to L02 cells (Figure 7B), which confirmed that cancer cells have higher metabolic activity and higher level of expression of the folate receptors on the cell surface.[61] The different responses of cancer cells in Figure 7B reflect the difference in the number of folate receptors per cell. The difference in the number of folate receptors per cell is related to the kinds of the cell lines[59] as well as size, morphology,[60] and cellular viability[61] of cell lines. Also, the level of folate receptors also appears to change at different stages of the cancer.[62,63] Since folate receptors are overexpressed on the cell membranes of different types of cancer cells, including ovarian, endometrial, colorectal, breast, lung, liver, kidney, prostate, renal cell carcinomas, brain metastases derived from epithelial cancers, neuroendocrine carcinomas, and so forth,[53,54,60] this method can be used for general cancer cell detection.

■ CONCLUSIONS

We reported the dual responsive enzyme mimetics based on CS-AgX nanomaterials, which showed enzyme mimetic activities toward classical chromogenic substrates, such as OPD, ABTS and TMB upon stimulation by H_2O_2 or visible-light. As a peroxdise mimetic (using H_2O_2 as an oxidant), they showed optimal activity in slightly acidic environments (pH 4.0) with their catalytic activity dependent on solution pH, temperature and H_2O_2 concentration. Upon visible-light photoactivation, they also exhibited excellent enzyme-like activity without H_2O_2. Kinetic analysis indicates that the activity of CS-AgX NPs stimulated by different manners shows the typical Michaelis−Menten kinetics and good affinity for TMB, which is superior to HRP in the same conditions. The photostimulated enzyme-like activity of AgX shows several unprecedented advantages over natural peroxidase or other existing alternatives based on nanomaterials. First, they exhibited excellent enzyme-like activity over a broad pH range (3.0−7.0), even at neutral pH. Second, the photostimulated oxidation of the substrate is independent of hydrogen peroxide in a fast manner (<10 min), introducing biocompatibility/effectiveness to the system. Furthermore, the photostimulated enzyme-like activity can be easily regulated by light irradiation and they can be reutilized without significant loss of catalytic activity. Here, we take advantage of the folic acid conjugated chitosan-AgI NPs to develop a facile, fast, and highly sensitive and selective colorimetric assay to detect cancer cells. We envision that the engineered catalytic AgX-based material with dual responsive enzyme-mimicking activity will hold great promise in potential applications, such as biocatalysts, biosensors, and so forth.

■ ASSOCIATED CONTENT

Supporting Information

Characterization of CS-AgI and folate-conjugated CS-AgI, catalytic oxidation of TMB by different CS-AgX catalysts and by different concentrations of CS-AgI, steady-state kinetic assay for CS-AgI, cycling runs of CS-AgI under visible light irradiation for the oxidation of TMB, and the catalytic mechanism of CS-AgI. This material is available free of charge via the Internet at http://pubs.acs.org/.

■ AUTHOR INFORMATION

Corresponding Author

*E-mail: glwang@jiangnan.edu.cn. Tel.:+86-510-85917090. Fax: +86-510-85917763.

Notes

The authors declare no competing financial interest.

■ ACKNOWLEDGMENTS

This work was supported by The National Natural Science Foundation of China (Nos. 21275065, 21005031), the Fundamental Research Funds for the Central Universities (JUSRP51314B), the MOE & SAFEA for the 111 Project (B13025), and the Opening Foundation of the State Key Laboratory of Analytical Chemistry for Life Science of Nanjing University (KLACLS1008).

■ REFERENCES

(1) Hult, K.; Berglund, P. Engineered Enzymes for Improved Organic Synthesis. *Curr. Opin. Biotechnol.* **2003**, *14*, 395−400.

(2) Barber, J. Photosynthetic Energy Conversion: Natural and Artificial. *Chem. Soc. Rev.* **2009**, *38*, 185−196.

(3) Liu, J.; Hu, X.; Hou, S.; Wen, T.; Liu, W.; Zhu, X.; Wu, X. Screening of Inhibitors for Oxidase Mimics of Au@Pt Nanorods by Catalytic Oxidation of OPD. *Chem. Commun.* **2011**, *47*, 10981−10983.

(4) Gao, L. Z.; Zhuang, J.; Nie, L.; Zhang, J. B.; Zhang, Y.; Gu, N.; Wang, T. H.; Feng, J.; Yang, D. L.; Perrett, S.; Yan, X. Intrinsic Peroxidase-Like Activity of Ferromagnetic Nanoparticles. *Nat. Nanotechnol.* **2007**, *2*, 577−583.

(5) Beslow, R. Biomimetic Chemistry and Artificial Enzymes: Catalysis by Design. *Acc. Chem. Res.* **1995**, *28*, 146−153.

(6) Song, Y. J.; Qu, K. G.; Zhao, C.; Ren, J. S.; Qu, X. G. Graphene Oxide: Intrinsic Peroxidase Catalytic Activity and its Application to Glucose Detection. *Adv. Mater.* **2010**, *22*, 2206−2210.

(7) Tao, Y.; Lin, Y.; Huang, Z. Z.; Ren, J. S.; Qu, X. Incorporating Graphene Oxide and Gold Nanoclusters: A Synergistic Catalyst with Surprisingly High Peroxidase-Like Activity Over a Broad pH Range and its Application for Cancer Cell Detection. *Adv. Mater.* **2013**, *25*, 2594−2599.

(8) Song, Y.; Wang, X. H.; Zhao, C.; Qu, K. G.; Ren, J. S.; Qu, X. G. Label-Free Colorimetric Detection of Single Nucleotide Polymorphism by Using Single-Walled Carbon Nanotube Intrinsic Peroxidase-Like Activity. *Chem.—Eur. J.* **2010**, *16*, 3617−3621.

(9) Cui, R. J.; Han, Z. D.; Zhu, J. J. Helical Carbon Nanotubes: Intrinsic Peroxidase Catalytic Activity and its Application for Biocatalysis and Biosensing. *Chem.—Eur. J.* **2011**, *17*, 9377−9384.

(10) Shi, W. B.; Wang, Q. L.; Long, Y. J.; Cheng, Z. L.; Chen, S. H.; Zheng, H. Z.; Huang, Y. M. Carbon Nanodots as Peroxidase Mimetics and their Applications to Glucose Detection. *Chem. Commun.* **2011**, *47*, 6695−6697.

(11) André, R.; Natálio, F.; Humanes, M.; Leppin, J.; Heinze, K.; Wever, R.; Schröder, H. C.; Müller, W. E. G.; Tremel, W. V_2O_5 Nanowires with an Intrinsic Peroxidase-Like Activity. *Adv. Funct. Mater.* **2011**, *21*, 501−509.

(12) Shi, W. B.; Zhang, X. D.; He, S. H.; Huang, Y. M. $CoFe_2O_4$ Magnetic Nanoparticles as a Peroxidase Mimic Mediated Chemiluminescence for Hydrogen Peroxide and Glucose. *Chem. Commun.* **2011**, *47*, 10785−10787.

(13) Mu, J. S.; Wang, Y.; Zhao, M.; Zhang, L. Intrinsic Peroxidase-Like Activity and Catalase-Like Activity of Co_3O_4 Nanoparticles. *Chem. Commun.* **2012**, *48*, 2540−2542.

(14) Jv, Y.; Li, B. X.; Cao, R. Positively-Charged Gold Nanoparticles as Peroxidiase Mimic and Their Application in Hydrogen Peroxide and Glucose detection. *Chem. Commun.* **2010**, *46*, 8017−8019.

(15) He, W. W.; Wu, X. C.; Liu, J. B.; Hu, X. N.; Zhang, K.; Hou, S.; Zhou, W.; Xie, S. Design of AgM Bimetallic Alloy Nanostructures(M = Au, Pd, Pt) with Tunable Morphology and Peroxidase-Like Activity. *Chem. Mater.* **2010**, *22*, 2988−2994.

(16) Wei, H.; Wang, E. Nanomaterials with Enzyme-Like Characteristics (Nanozymes): Next-Generation Artificial Enzymes. *Chem. Soc. Rev.* **2013**, *42*, 6060−6093.

(17) He, W. W.; Liu, Y.; Yuan, J. S.; Yin, J. J.; Wu, X. C.; Hu, X. N.; Zhang, K.; Liu, J. B.; Chen, C. Y.; Ji, Y. L.; Guo, Y. T. Au@Pt Nanostructures as Oxidase and Peroxidase Mimetics for Use in Immunoassays. *Biomaterials* **2011**, *32*, 1139−1147.

(18) Liu, X.; Wang, Qi.; Zhao, H. H.; Zhang, L. C.; Su, Y. Y.; Lv, Y. BSA-Templated MnO_2 Nanoparticles as Both Peroxidase and Oxidase Mimics. *Analyst* **2012**, *137*, 4552−4558.

(19) Wang, H. W.; Jiang, W. W.; Wang, Y. W.; Liu, X. L.; Yao, J. L.; Yuan, L.; Wu, Z. Q.; Li, D.; Song, B.; Chen, H. Catalase-Like and Peroxidase-Like Catalytic Activities of Silicon Nanowire Arrays. *Langmuir* **2013**, *29*, 3−7.

(20) Cook, C. J. Real-Time Measurements of Corticosteroids in Conscious Animals Using an Antibody-Based Electrode. *Nat. Biotechnol.* **1997**, *15*, 467−471.

(21) van der Want, J. J.; Klooster, J.; Cardozo, B. N.; de Weerd, H.; Liem, R. S. Tract-Tracing in the Nervous System of Vertebrates Using Horseradish Peroxidase and its Conjugates: Tracers, Chromogens and Stabilization for Light and Electron Microscopy. *Brain Res. Protoc.* **1997**, *1*, 269−279.

(22) Schauer, C. L.; Chen, M. S.; Chatterley, M.; Eisemann, K.; Welsh, E. R.; Price, R. R.; Schoen, P. E.; Ligler, F. S. Color Changes in Chitosan and Poly(allyl amine) Films upon Metal Binding. *Thin Solid Films* **2003**, *434*, 250−257.

(23) Laudenslager, M. J.; Schiffman, J. D.; Schauer, C. L. Carboxymethyl Chitosan as a Matrix Material for Platinum, Gold, and Silver Nanoparticles. *Biomacromolecules* **2008**, *9*, 2682−2685.

(24) Jang, G. G.; Roper, D. K. Balancing Redox Activity Allowing Spectrophotometric Detection of Au(I) Using Tetramethylbenzidine Dihydrochloride. *Anal. Chem.* **2011**, *83*, 1836−1842.

(25) Ali, M.; Tahir, M. N.; Siwy, Z.; Neumann, R.; Tremel, W.; Ensinger, W. Hydrogen Peroxide Sensing with Horseradish Peroxidase-Modified Polymer Single Conical Nanochannels. *Anal. Chem.* **2011**, *83*, 1673−1680.

(26) Wang, X. X.; Wu, Q.; Shan, Z.; Huan, Q. M. BSA-Stabilized Au Clusters as Peroxidase Mimetics for Use in Xanthine Detection. *Biosens. Bioelectron.* **2011**, *26*, 3614−3619.

(27) Zhang, Z. X.; Wang, X. L.; Yang, X. R. A Sensitive Choline Biosensor Using Fe_3O_4 Magnetic Nanoparticles as Peroxidase Mimics. *Analyst* **2011**, *136*, 4960−4965.

(28) Michaelis, L.; Menten, M. L. Die Kinetik der Invertinwirkung. *Biochem. Z.* **1913**, *49*, 333−369.

(29) Cai, K.; Lv, Z. C.; Chen, K.; Huang, L.; Wang, J.; Shao, F.; Wang, Y. J.; Han, H. Y. Aqueous Synthesis of Porous Platinum Nanotubes at Room Temperature and Their Intrinsic Peroxidase-Like Activity. *Chem. Commun.* **2013**, *49*, 6024−6026.

(30) Wang, W.; Jiang, X. P.; Chen, K. Z. Iron Phosphate Microflowers as Peroxidase Mimic and Superoxide Dismutase Mimic for Biocatalysis and Biosensing. *Chem. Commun.* **2012**, *48*, 7289−7291.

(31) An, C. H.; Wang, J. Z.; Qin, C.; Jiang, W.; Wang, S. T.; Li, Y.; Zhang, Q. H. Synthesis of Ag@AgBr/AgCl Heterostructured Nanocashews with Enhanced Photocatalytic Performance via Anion Exchange. *J. Mater. Chem.* **2012**, *22*, 13153−13158.

(32) Cao, J.; Xu, B. Y.; Luo, B. D.; Lin, H. L.; Chen, S. F. Preparation, Characterization and Visible-Light Photocatalytic Activity of AgI/AgCl/TiO_2. *Appl. Surf. Sci.* **2011**, *257*, 7083−7089.

(33) Ishibashi, K.; Fujishima, A.; Watanabe, T.; Hashimoto, K. Quantum Yields of Active Oxidative Species Formed on TiO_2 Photocatalyst. *J. Photochem. Photobiol., A* **2000**, *134*, 139−142.

(34) Anastasios, I.; Mitsionis, T. C.; Vaimakis. The Effect of Thermal Treatment in TiO_2 Photocatalytic Activity. *J. Therm. Anal. Calorim.* **2013**, *112*, 621−628.

(35) Hayon, E.; Simic, M. Acid-Base Properties of Free Radicals in Solution. *Acc. Chem. Res.* **1974**, *7*, 114−121.

(36) Manring, L. E.; Kramer, M. K. Interception of O_2^- by Benzoquinone in Cyanoaromatic-Sensitized Photooxygenations. *Tetrahedron Lett.* **1984**, *25*, 2523−2526.

(37) Niu, P.; Hao, J. C. Fabrication of Titanium Dioxide and Tungstophosphate Nanocomposite Films and Their Photocatalytic Degradation for Methyl Orange. *Langmuir* **2011**, *27*, 13590−13597.

(38) Li, W. J.; Li, D. Z.; Xian, J. J.; Chen, W.; Hu, Y.; Shao, Y.; Fu, X. Z. Specific Analyses of the Active Species on $Zn_{0.28}Cd_{0.72}S$ and TiO_2 Photocatalysts in the Degradation of Methyl Orange. *J. Phys. Chem. C* **2010**, *114*, 21482−21492.

(39) Shah, V.; Verma, P.; Stopka, P.; Gabriel, J.; Baldrian, P.; Nerud, F. Decolorization of Dyes with Copper(II)/Organic Acid/Hydrogen Peroxide Systems. *Appl. Catal., B* **2003**, *46*, 287−292.

(40) Liu, R. H.; Fu, S. Y.; Zhan, H. Y.; Lucia, L. A. General Spectroscopic Protocol to Obtain the Concentration of the Superoxide Anion Radical. *Ind. Eng. Chem. Res.* **2009**, *48*, 9331−9334.

(41) Feng, S.; Xu, H.; Liu, L.; Song, Y. H.; Li, H. M.; Xu, Y. G.; Xia, J. X.; Yin, S.; Yan, J. Controllable Synthesis of Hexagon-Shaped β-AgI Nanoplates in Reactable Ionic Liquid and Their Photocatalytic Activity. *Colloids Surf., A* **2012**, *410*, 23−30.

(42) Cheng, H. F.; Huang, B. B.; Dai, Y.; Qin, X. Y.; Zhang, X. Y. One-Step Synthesis of the Nanostructured AgI/BiOI Composites with Highly Enhanced Visible-Light Photocatalytic Performances. *Langmuir* **2010**, *26*, 6618−6624.

(43) Jiang, J.; Zhang, X.; Sun, P. B.; Zhang, L. Z. ZnO/BiOI Heterostructures: Photoinduced Charge-Transfer Property and Enhanced Visible-Light Photocatalytic Activity. *J. Phys. Chem. C* **2011**, *115*, 20555−20564.

(44) Meng, F.; Li, J. T.; Cushing, S. K.; Zhi, M. J.; Wu, N. Q. Solar Hydrogen Generation by Nanoscale p−n Junction of p-Type Molybdenum Disulfide/n-Type Nitrogen-Doped Reduced Graphene Oxide. *J. Am. Chem. Soc.* **2013**, *135*, 10286−10289.
(45) Kuvarega, A. T.; Krause, R. W. M.; Mamba, B. B. Nitrogen/Palladium-Codoped TiO_2 for Efficient Visible Light Photocatalytic Dye Degradation. *J. Phys. Chem. C* **2011**, *115*, 22110−22120.
(46) Kibombo, H. S.; Koodali, R. T. Heterogeneous Photocatalytic Remediation of Phenol by Platinized Titania-Silica Mixed Oxides Under Solar-Simulated Conditions. *J. Phys. Chem. C* **2011**, *115*, 25568−25579.
(47) Xu, L.; Steinmiller, E. M. P.; Skrabalak, S. E. Achieving Synergy with a Potential Photocatalytic Z-Scheme: Synthesis and Evaluation of Nitrogen-Doped TiO_2/SnO_2 Composites. *J. Phys. Chem. C* **2012**, *116*, 871−877.
(48) Zhong, H.; Zhang, Q.; Zhang, S. High-Intensity Fluorescence Imaging and Sensitive Electrochemical Detection of Cancer Cells by Using an Extracellular Supramolecular Reticular DNA-Quantum Dot Sheath. *Chem.—Eur. J.* **2011**, *17*, 8388−8394.
(49) Song, Y. J.; Chen, Y.; Feng, L. Y.; Ren, J. S.; Qu, X. G. Selective and Quantitative Cancer Cell Detection Using Target-Directed Functionalized Graphene and its Synergetic Peroxidase-Like Activity. *Chem. Commun.* **2011**, *47*, 4436−4438.
(50) Feng, L. Y.; Chen, Y.; Ren, J. S.; Qu, X. G. A Graphene Functionalized Electrochemical Aptasensor for Selective Label-Free Detection of Cancer Cells. *Biomaterials* **2011**, *32*, 2930−2937.
(51) Wu, L.; Wang, J. S.; Ren, J. S.; Li, Wen.; Qu, X. G. Highly Sensitive Electrochemiluminescent Cytosensing Using Carbon Nano-dot@Ag Hybrid Material and Graphene for Dual Signal Amplification. *Chem. Commun.* **2013**, *49*, 5675−5677.
(52) Kohler, N.; Sun, C.; Wang, J.; Zhang, M. Q. Methotrexate-Modified Superparamagnetic Nanoparticles and Their Intracellular Uptake into Human Cancer Cells. *Langmuir* **2005**, *21*, 8858−8864.
(53) Zhao, M. X.; Huang, H. F.; Xia, Q.; Ji, L. N.; Mao, Z. W. γ-Cyclodextrin-Folate Complex-Functionalized Quantum Dots for Tumor-Targeting and Site-Specific Labeling. *J. Mater. Chem.* **2011**, *21*, 10290−10297.
(54) Bharali, D. J.; Lucey, D. W.; Jayakumar, H.; Pudavar, H. E.; Prasad, P. N. Folate-Receptor-Mediated Delivery of InP Quantum Dots for Bioimaging Using Confocal and Two-Photon Microscopy. *J. Am. Chem. Soc.* **2005**, *127*, 11364−11371.
(55) Asati, A.; Santra, S.; Kaittanis, C.; Nath, S.; Perez, J. M. Oxidase-Like Activity of Polymer-Coated Cerium Oxide Nanoparticles. *Angew. Chem., Int. Ed.* **2009**, *48*, 2308−2312.
(56) Scheller, F. W.; Bauer, C. G.; Makower, A.; Wollenberger, U.; Warsinke, A.; Bier, F. F. In *Biomolecular Sensors*, 1st ed.; Gizeli, E., Lowe, C L., Eds.; Taylor & Francis Ltd.: New York, 2002; Chapter 8, pp 207−238.
(57) Warsinke, A. Electrochemical Biochips for Protein Analysis. *Adv. Biochem. Eng. Biotechnol.* **2008**, *109*, 155−193.
(58) Yang, H. Enzyme-Based Ultrasensitive Electrochemical Biosensors. *Curr. Opin. Chem. Biol.* **2012**, *16*, 422−428.
(59) Asati, A.; Kaittanis, C.; Santra, S.; Perez, J. M. pH-Tunable Oxidase-Like Activity of Cerium Oxide Nanoparticles Achieving Sensitive Fluorigenic Detection of Cancer Biomarkers at Neutral pH. *Anal. Chem.* **2011**, *83*, 2547−2553.
(60) Song, Y. C.; Shi, W.; Chen, W.; Li, X. H.; Ma, H. M. Fluorescent Carbon Nanodots Conjugated with Folic Acid for Distinguishing Folate-Receptor-Positive Cancer Cells from Normal Cells. *J. Mater. Chem.* **2012**, *22*, 12568−12573.
(61) Rosenholm, J. M.; Meinander, A.; Peuhu, E.; Niemi, R.; Eriksson, J. E.; Sahlgren, C.; Lindén, M. Targeting of Porous Hybrid Silica Nanoparticles to Cancer Cells. *ACS Nano* **2009**, *3*, 197−206.
(62) Lu, Y. J.; Low, P. S. Folate-Mediated Delivery of Macro-molecular Anticancer Therapeutic Agents. *Adv. Drug Delivery Rev.* **2002**, *54*, 675−693.
(63) Toffoli, G.; Russo, A.; Gallo, A.; Cernigoi, C.; Miotti, S.; Sorio, R. Expression of Folate Binding Protein as a Prognostic Factor for Response to Platinum-Containing Chemotherapy and Survival in Human Ovarian Cancer. *Int. J. Cancer* **1998**, *79*, 121−126.